16th World Conference on Earthquake, 16WCEE 2017

Santiago Chile, January 9th to 13th 2017

Paper N° 386

Registration Code: S-Y1462954717

Simulation-based probabilistic tsunami hazard analysis for near-field seismic sources: application to the Tohoku region, Japan.

R. De Risi[(1)], K. Goda[(2)]

[(1)] Research Associate, Department of Civil Engineering, University of Bristol, raffaele.derisi@bristol.ac.uk
[(2)] Senior Lecturer, Department of Civil Engineering, University of Bristol, katsu.goda@bristol.ac.uk

Abstract

Probabilistic tsunami hazard analysis is the fundamental prerequisite for rigorous risk assessment and thus for decision-making regarding mitigation strategies. The analysis involves numerous uncertain parameters that are related to geophysical processes (e.g. slip rate, slip distribution, and dip), potential sea conditions (e.g. tidal level), and inundation processes (e.g. roughness and topography). A comprehensive treatment of these uncertainties is challenging due to the lack of high-resolution/accuracy data and the great computational effort involved in tsunami simulation.

A simulation-based procedure to estimate the likelihood that tsunami inundation at particular location will exceed a given level, within a certain period of time, is presented. Key features of existing hazard assessment methodologies, such as worst-case scenario, sensitivity analysis, and probabilistic hazard analysis, are combined to develop a new procedure for probabilistic tsunami hazard assessment for near-field seismic sources. To reduce the computational efforts and to focus on the methodological aspect, only a specific seismogenic context, i.e. near-field sources in the Tohoku region of Japan, is taken into account. Nevertheless, the procedure can be extended to consider all possible sources of interest for the Tohoku region and can be applied to other subduction zones. Furthermore, only geophysical uncertainty is considered herein; notwithstanding such limitations, the simulation-based procedure facilitates the implementation of all other sources of uncertainties in a straightforward manner.

After the selection of a tsunami occurrence model, the first step of the procedure is the definition of a magnitude-frequency distribution of major tsunami events; this function is then used to calculate the annual rate of exceedance of major tsunami events. For a given value of earthquake magnitude, size and geometry of the rupture area are determined using new empirical scaling relationships, bespoke for subduction areas. In this step, both aleatory and epistemic uncertainties of model parameters (i.e. position, length, width, strike, and dip) can be incorporated based on the probabilistic information available in the literature. In particular, multiple realizations of possible earthquake slip distributions are generated using a spectral synthesis method. The incorporation of the stochastic slip models in probabilistic tsunami hazard analysis is novel with respect to the previous studies; conventionally, slip distributions within a fault rupture plane are considered as uniform or randomly distributed (without realistic spatial distribution of the slip).

Subsequently, for each generated slip distribution, the seafloor vertical displacement is calculated using analytical formulae and tsunami simulation is performed by solving nonlinear shallow water equations. By repeating the above procedure for numerous tsunami scenarios, the empirical distribution of the maximum wave heights and velocities (i.e. intensity measures) can be obtained for rigorous tsunami hazard analysis. The minimum number of simulations required to obtain stable estimates of tsunami intensity measures, especially the higher percentiles, is investigated through a statistical bootstrap analysis.

The site-specific tsunami hazard curve can be derived by integrating the annual occurrence rates of the tsunami events and their tsunami inundation results. The results are particularly useful for tsunami hazard mapping purposes and the developed framework can be further extended to probabilistic tsunami risk analysis using tsunami fragility models.

Keywords: Probabilistic Tsunami Hazard Analysis; magnitude-frequency relationship; scaling relationships of earthquake source parameters; stochastic rupture models.

1. Introduction

Tsunamis are catastrophic events triggered by different potential natural causes, such as seismic events, volcanic eruptions, submarine landslides, and asteroid/meteorite impacts. In the last two and a half centuries, more than 2500 major tsunami events occurred around the world [1], and submarine earthquakes triggered more than a half of those events. Therefore, in this study, tsunami events generated by seismic events are focused on. To evaluate the performance of critical facilities and urban infrastructure and to develop viable risk mitigation strategies against large tsunamis, rigorous probabilistic hazard analysis is essential. Moreover, enhancing preparedness and resilience against future tsunami disasters is critical for sustainable development of coastal areas.

There are mainly three methodologies for tsunami hazard assessment in the literature [2]: (a) probabilistic tsunami hazard analysis (PTHA), (b) worst-case scenario approach, typically a deterministic method used for the development of practical emergency management products, such as evacuation maps and coastal infrastructure design [3], and (c) sensitivity analysis, where the most influential model parameters are identified [4,5]. The existing PTHA can be classified into three categories. In the first category, PTHA is conducted by using tsunami catalogs [6-8], whereas in the second category, different "scenario-based" PTHA methods are suggested [9-11]. In the third category, a combination of the two previous categories is considered [12]. PTHA has many common features with probabilistic seismic hazard analysis (PSHA, [13]). Nevertheless, prior to the 2004 Sumatra event only several studies treated the tsunami hazard probabilistically [14-17]. After that event, the number of probabilistic tsunami hazard studies has increased rapidly [18-22], facilitated by the availability of simulation codes and computational resources.

This study presents a new PTHA methodology for near-field seismic sources. This methodology focuses on the near-sources in order to reduce the computational effort; however, it can be extended to consider all possible sources in the area and can be applied to other subduction zones. The proposed methodology overcomes some of the previous limitations, such as inappropriate scaling relationships of source parameters, unrealistic slip distributions, subjective weights of the logic-tree branches, and simplified inundation models. The first step is to define a tsunami occurrence model. In this study, a classical Poisson model is adopted. Assuming a Poissonian arrival time process, the probability of occurrence of a tsunami with specific characteristics in a given time window depends on the mean annual occurrence rate alone. Then, a magnitude-frequency distribution of major seismic events that may trigger tsunamis is defined. For discrete values of magnitude (i.e. 7.5, 7.75, 8.0, 8.25, 8.5, 8.75, and 9.0), it is possible to determine the characteristics of the rupture geometry and slip distribution using empirical scaling relationships of earthquake source parameters for subduction zones. The source parameters considered include fault length and width, mean and maximum slip, the Hurst number, and the correlation lengths along dip and strike. Therefore, for each value of magnitude, multiple realizations of possible earthquake slip distribution can be generated by adopting the von Kármán model as wavenumber spectrum [23].

For stochastic tsunami simulation, the subduction plane is discretized into sub-faults of 10-km by 10-km, and for each sub-fault, the seafloor displacement corresponding to 1 m of slip is calculated using analytical equations by Okada [24] and Tanioka and Satake [25]. For each simulated earthquake slip (i.e. event), the overall seafloor displacement field is estimated by scaling and summing the seafloor deformation fields of all individual sub-faults that make up the event. For each slip distribution, the tsunami simulation is performed by solving non-linear shallow water equations [26]. By repeating the simulation a sufficient number of times, samples of maximum tsunami wave heights and velocities at a location of interest can be obtained for each magnitude. The sufficient number of simulations for a specific value of magnitude is investigated through a bootstrap procedure. For each magnitude, the results obtained from the simulations are used to build the empirical complementary cumulative density function (CCDF), representing the conditional probability of reaching or exceeding a given intensity measure value. Such an empirical CCDF is obtained as the Kaplan-Meier estimator [27], for which the variance can be calculated through the Greenwood's formula [28], and therefore a confidence interval around the central estimate can be obtained.

The site-specific tsunami hazard curve can be derived by integrating the tsunami simulation results and the magnitude-frequency distribution for the discrete values of magnitude, and multiplying the result by the occurrence rate of earthquakes from the subduction fault. The result will be a triplet of empirical CCDFs (central estimate and confidence interval curves) representing the mean annual rate of exceedance of a given value of tsunami hazard parameter. To demonstrate the developed methodology, the procedure is applied to the Tohoku region, Japan, where the subduction fault plane is well defined from previous studies [5] and information on regional seismicity is available. Specifically, the hazard for a point located on the coastline of the City of Sendai, Miyagi Prefecture, is calculated.

2. Methodology

Let *IM* represent the tsunami intensity measure of interest, such as inundation height (*h*) or flow velocity (*v*); assuming a Poissonian arrival time process, the probability to observe the first occurrence of a tsunami having intensity value equal or greater than the specific value *im* in *t* years is:

$$P\left(IM \geq im \mid t\right) = 1 - \exp\left[-\lambda\left(IM \geq im\right)\cdot t\right] \tag{1}$$

where $\lambda(IM \geq im)$ is the mean annual rate at which the tsunami intensity measure *IM* will exceed the specific value *im*, at a given location. In analogy to the methodology by Parsons and Geist [21] for the probabilistic assessment of tsunami run-up, the rate $\lambda(IM \geq im)$ can be described as a filtered Poisson process:

$$\lambda\left(IM \geq im\right) = \lambda\left(M_W \geq M_{W,min}\right)\cdot\int P\left(IM \geq im \mid \boldsymbol{\theta}\right)\cdot S\left(\boldsymbol{\theta} \mid M_W\right)\cdot f\left(M_W\right)\cdot dM_W \tag{2}$$

where $\lambda(M_W \geq M_{W,min})$ is the mean annual rate of occurrence of the seismic event triggering a tsunami with magnitude greater than the minimum magnitude considered in the magnitude-frequency distribution for the zone analyzed. $P(IM \geq im|\boldsymbol{\theta})$ is the probability that the tsunami intensity measure *IM* will exceed a prescribed value *im* at a given coastal location for a given set of tsunami source parameters $\boldsymbol{\theta}$. The term $S(\boldsymbol{\theta}|M_W)$ represents the functional distribution of the uncertain source parameters conditioned on the earthquake magnitude. Finally, $f(M_W)$ is the magnitude-frequency distribution.

Fig. 1 shows a graphical representation of the proposed methodology. Five phases are defined: (i) definition of input data (i.e. magnitude-frequency distribution, fault model, and scaling relationships), (ii) stochastic source model generation, (iii) tsunami modeling, (iv) statistical analysis of simulated tsunami results, and (v) final convolution. Descriptions for each of these phases are presented in the following.

2.1 Magnitude-frequency distribution

In this study, a truncated Gutenberg-Richter relationship [29] is adopted, considering the interval of magnitude [7.375÷9.125]. For the analyzed Tohoku case study, a *b*-value equal to 0.9 [30] is adopted. The minimum magnitude value is chosen, since small-to-moderate earthquakes rarely generate significant tsunamis and their contribution to the tsunami hazard is negligible [18]. Fig. 1 (panel *a*) shows the case specific magnitude-frequency distribution (red line) that is also compared with the classical Gutenberg-Richter curve (black line) and with the tapered Gutenberg-Richter (blue line). For the simulation, it is convenient to convert the continuous distribution of magnitudes into a discrete set of magnitudes. A discretization interval of 0.25 is adopted, and therefore seven values of moment magnitude are analyzed (i.e. 7.5, 7.75, 8.0, 8.25, 8.5, 8.75, and 9.0). Fig. 1 (panel *a*) also shows the conditional probabilities of occurrence of these discrete magnitudes.

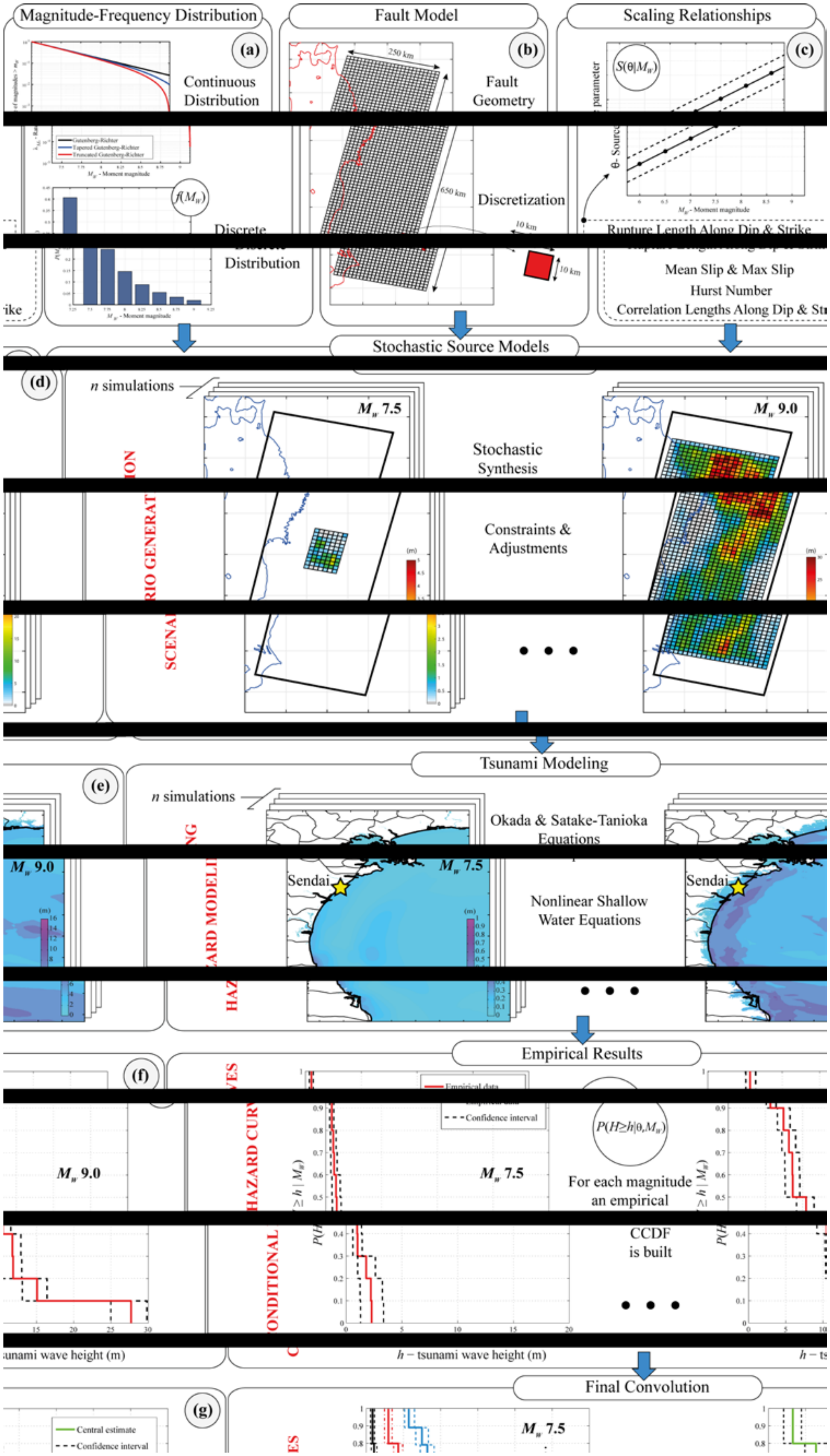

Fig. 1 – Computational framework for the PTHA

2.2 Fault model

A Tohoku-type fault is analyzed with an extension of 650 km along the strike and 250 km along the dip (panel *b* in Fig. 1); this is the extended fault plane of the source model by Satake et al. [31]. The fault model can accommodate a M_W9-class earthquake, consistent with the maximum magnitude adopted for the magnitude-frequency distribution. The stochastic synthesis of simulated seismic events requires a discretization into many sub-faults, therefore a 10-km mesh with variable dip is generated based on Satake et al. [31]. Such discretization allows modeling accurately the slip distribution corresponding to a M_W7.5 seismic event (i.e. the smallest central discrete value of moment magnitude), involving at least 5 by 5 sub-faults.

Once the major area containing all possible rupture scenarios is defined, the mean annual rate of occurrence of earthquakes with magnitude greater than or equal to 7.375 falling in that area can be calculated. In order to perform such a calculation, the NEIC earthquake catalog[1] is used. Fig. 2 (a) shows the events reported in the database that fall in the considered major rupture area, recorded in the period 1976-2012, having a depth varying between 0 km and 60 km, and considering a magnitude range between 5 and 9. The rate estimate $\lambda(M_W \geq 7.375)$ is equal to 0.183.

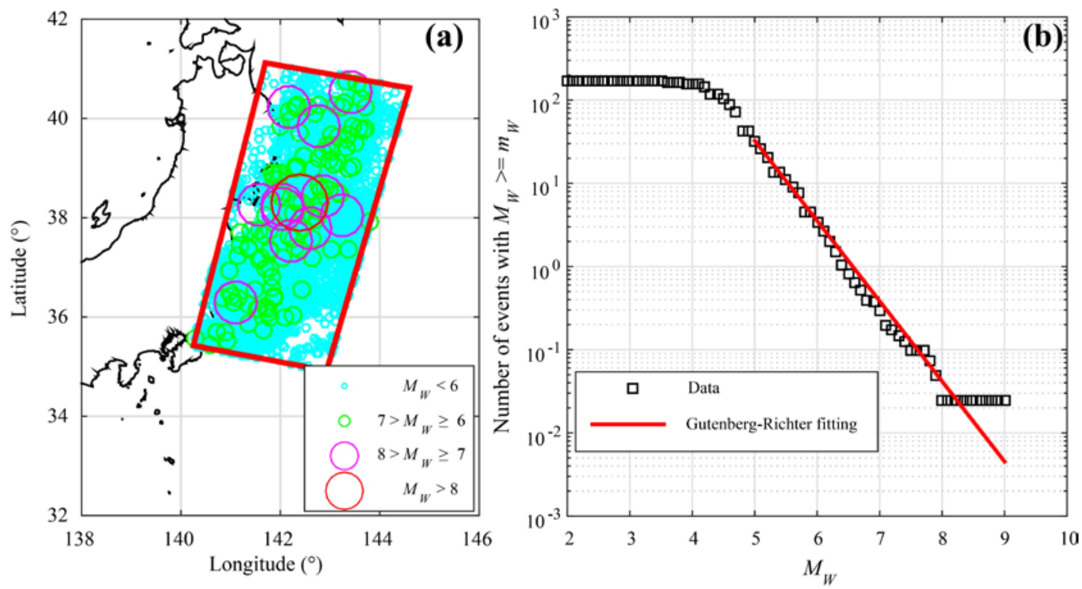

Fig. 2 – (a) NEIC catalog, and (b) magnitude-frequency representation.

2.3 Scaling relationships of earthquake source parameters and stochastic source models

A certain number of stochastic source models is simulated (panel *d* in Fig. 1) to take into account aleatory uncertainties related to the rupture process. The simulation procedure is based on the spectral synthesis method [5, 32], characterizing the earthquake slip distribution by wavenumber spectra [23]. Herein, scaling relationships that evaluate the source parameters (e.g. rupture size and spectral characteristics of the rupture) are used for stochastic tsunami simulation as a function of moment magnitude. Such scaling relationships are obtained on the basis of 226 inverted source models in the SRCMOD database [33]. The details of the adopted models can be found in Goda et al. [34]. It is important to emphasize that a correlation structure among the source parameters is also considered.

[1] http://earthquake.usgs.gov/earthquakes/search/

2.4 Tsunami modeling

For each stochastic event, the maximum inundation intensity measure for a specific location is computed (panel *e* in Fig. 1). The initial water surface elevation for an earthquake slip model is evaluated using analytical formulae for elastic dislocation by Okada [24] together with the equation by Tanioka and Satake [25]. The latter is to take into account the effects of horizontal movements of steep seafloor on the vertical water dislocation. To optimize the seafloor dislocation computation, the seafloor displacement field induced by a unity slip for each sub-fault is computed in advance. Then to obtain the effects of the i^{th} slip distribution, each displacement field is scaled and summed to reflect the i^{th} simulated event.

Tsunami modeling is then carried out using a well-tested numerical code of Goto et al. [26] that is capable of generating offshore tsunami propagation and inundation profiles by evaluating non-linear shallow water equations with run-up using a leapfrog staggered-grid finite difference scheme. The run-up calculation is based on a moving boundary approach, where a dry/wet condition of a computational cell is determined based on total water depth relative to its elevation. The numerical tsunami calculation is performed for 2 hours which is sufficient to model the most critical phases of tsunami waves. The integration time step is determined by satisfying the C.F.L. condition; it depends on the bathymetry/elevation data and their grid sizes and is typically between 0.1 s and 0.5 s. Through this code, it is possible to obtain the maximum tsunami intensity measures of interest (i.e. tsunami height, tsunami velocity, etc.) for one or more specific locations along the coast. The results can also be used to evaluate aggregate tsunami hazard parameters, such as inundation areas above a certain depth.

A complete dataset of bathymetry/elevation, coastal/riverside structures (e.g. breakwater and levees), and surface roughness is obtained from the Miyagi prefectural government. The data are provided in the form of nested grids (1350-m – 450-m – 150-m – 50-m), covering the geographical regions of Tohoku. The ocean-floor topography data are based on the 1:50,000 bathymetric charts and JTOPO30 database developed by the Japan Hydrographic Association and based on the nautical charts developed by the Japan Coastal Guard. The tidal fluctuation is not taken into account in this study. The elevation data of the coastal/riverside structures are primarily provided by municipalities. In the tsunami simulation, the coastal/riverside structures are represented by a vertical wall at one or two sides of the computational cells. To evaluate the volume of water that overpasses these walls, Honma's overflowing formulae are employed. In the tsunami simulation, the bottom friction is evaluated using Manning's formula. The Manning's coefficients are assigned to computational cells based on national land use data in Japan: 0.02 $m^{-1/3}s$ for agricultural land, 0.025 $m^{-1/3}s$ for ocean/water, 0.03 $m^{-1/3}s$ for forest vegetation, 0.04 $m^{-1/3}s$ for low-density residential areas, 0.06 $m^{-1/3}s$ for moderate-density residential areas, and 0.08 $m^{-1/3}s$ for high-density residential areas.

2.5 Empirical representation of the tsunami simulation results

For each value of magnitude, the simulations are used to build the term $P(IM \geq im|M_W)$ for the locations of interest. Such probability is represented by the empirical CCDF of the resulting empirical *IM* (panel *f* in Fig. 1). Specifically, the empirical *IM* is represented as the Kaplan-Meier estimator [27], being the hazard central estimate. In addition, a confidence interval around the central estimate can be represented, calculating the variance of the empirical data through the Greenwood's formula [28]. In this study, the 95% confidence interval is considered.

2.6 Hazard assessment

The empirical curves obtained in the previous step for each magnitude are then multiplied by the probability corresponding to the related magnitude, and eventually are summed up (panel *g* in Fig. 1). Also in this phase, three curves are obtained, one corresponding to the central value and two for the confidence interval. The final hazard curves, representing the mean annual rate of occurrence of a specific value of tsunami intensity measure, are obtained by multiplying the previous three functions by the rate of occurrence of events with magnitudes greater than the minimum magnitude considered in the magnitude-frequency distribution.

3. Results

Two main results are presented: (a) the minimum number of simulations in order to obtain a reliable assessment of the intensity measure of interest, and (b) the hazard curve for Sendai (see the star symbol in panel *e* of Fig. 1) obtained using the proposed methodology.

3.1 Effects of the number of simulations

A short or incomplete empirical record leads to biased estimation of the hazard parameters, especially when conventional statistical methods are used [35]. To understand the effect of the number of simulations on the final hazard estimation, a bootstrap procedure is carried out. In general, bootstrap is performed by randomly sampling, through a Monte Carlo simulation, i.e. m values from the original sample containing n elements (with $m \leq n$). This provides a pool of different samples of independent and identically distributed random variables with the distribution function equal to the empirical distribution function of the original sample. For each generated sample, an estimate of the parameter of interest (e.g. mean, median, and different percentiles) is then computed. The ensemble of such estimates can be used to identify the uncertainty in the parameter value.

Fig. 3 shows five percentiles (i.e. 5th, 25th, 50th, 75th, and 95th) of the wave height calculated at the Sendai coast for different magnitude values (i.e. 7.5, 8.0, 8.5, and 9.0) as a function of the number of simulations. The analysis is carried out considering a fixed original sample of n = 500 simulations. The bootstrap procedure is then applied considering the number of simulations m varying between 1 and 500; for each trial number of simulations m, 1000 Monte Carlo samples are realized. The curves are then obtained as the mean value of such simulations. The results show that the central estimates (i.e. the 50th percentile, represented with the black line) is stable after 100 simulations for all the considered magnitude values. To obtain stable high percentiles, a larger number of simulations are needed (the red dotted line in Fig. 3). In particular, 300 simulations are necessary for M_W7.5, 250 simulations for M_W8.0, and 200 simulations for M_W8.5 and M_W9.0. Such a decreasing trend with the magnitude is consistent with the physical process: when the magnitude is relatively small, the rupture area can move more freely over the fault plane (see panel *d* in Fig. 1), increasing the variability on the inundation intensity measures. In turn, when the magnitude is large, the fluctuation of the rupture area is more constrained (i.e. the major slip area tends to occupy the entire subduction plane).

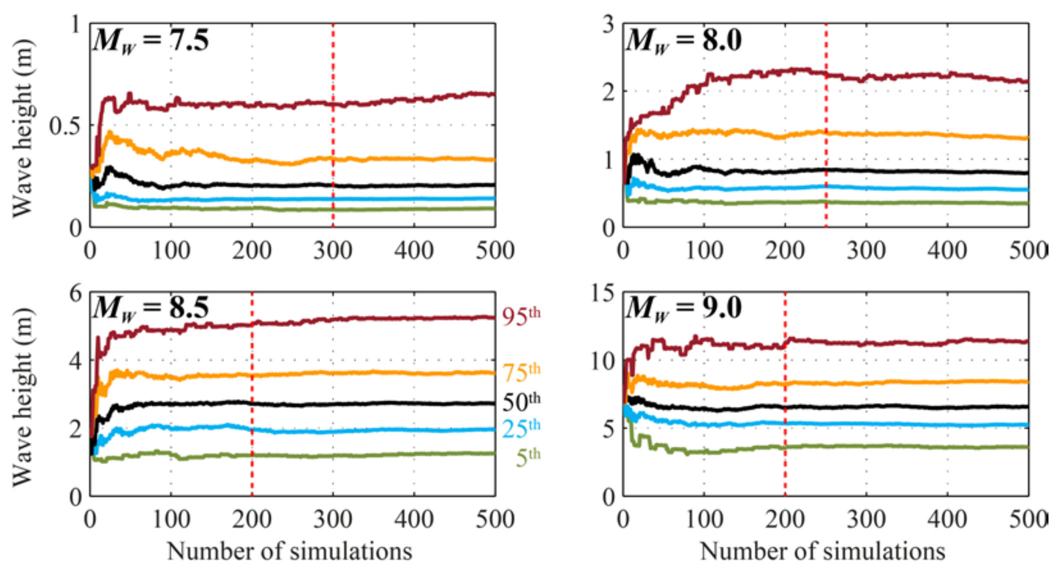

Fig. 3 – Wave height percentiles for different values of magnitude as a function of the number of simulations

3.2 Tsunami hazard curves

For each value of seven magnitudes (i.e. 7.5, 7.75, 8.0, 8.25, 8.5, 8.75, and 9.0), 300 sets of the tsunami source parameters $\boldsymbol{\theta}$ are generated using the scaling relationships by Goda et al. [34]. Fig. 4 shows, as an example, the scaling relationships for the rupture length and width (Fig. 4 (a) and (b)), and for mean and maximum slip (Fig. 4 (c) and (d)). On the same plots, simulated data (green dots) and associated statistics (colored circles) are also shown. Simulated data are in agreement with the source parameter distributions (i.e. green dots are well clustered within the confidence interval of the scaling models). Magnitude values of the simulated data are not perfectly aligned at the seven discrete values; in fact, the simulation algorithm allows a tolerance band of ±0.05 around each magnitude value.

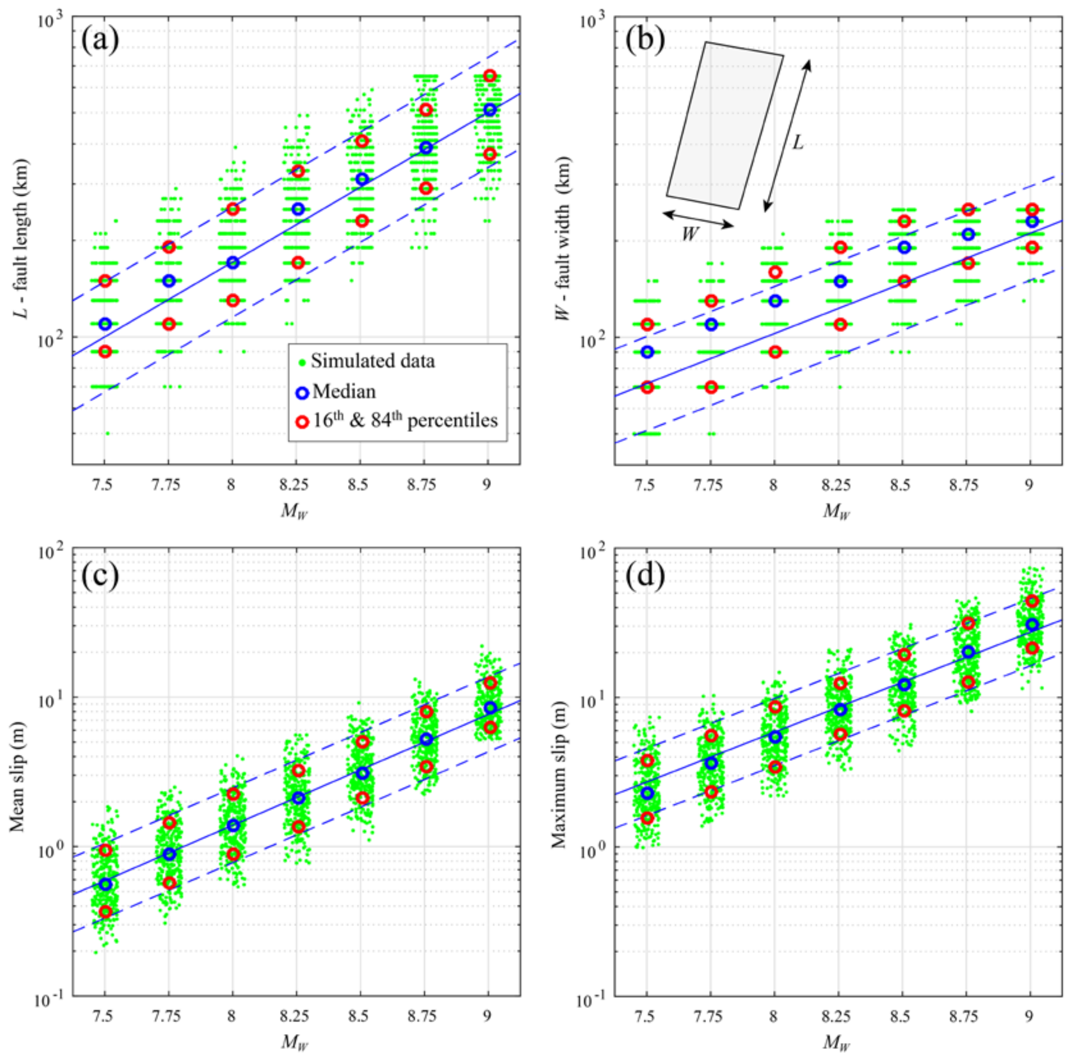

Fig. 4 – Scaling relationships for the (a) rupture length, (b) rupture width, (c) mean slip, and (d) maximum slip. The simulated values (green dots) and the corresponding percentiles (colored circles) are also shown.

Then, for each discrete magnitude value, 300 tsunami simulations are performed. The empirical CCDFs in terms of tsunami wave height for Sendai are presented in Fig. 5 (a) for all the magnitude values analyzed. Fig. 5 (b) shows the same curves, weighted by the probability values obtained from the discretized Gutenberg-Richter relationship. As shown in the panel *g* of Fig. 1, the summation of the curves presented in Fig. 5 (b), multiplied by $\lambda(M_W \geq 7.375) = 0.183$ (Fig. 2), leads to the final hazard curves (Fig. 6).

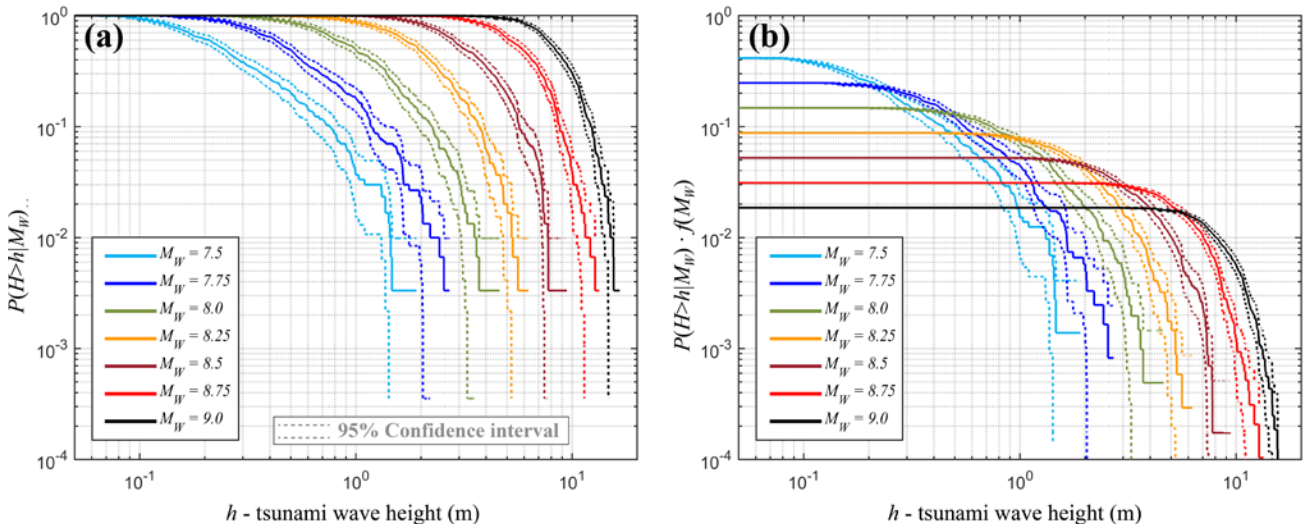

Fig. 5 – (a) Conditional probability and (b) weighted conditional probability of exceedance of a specific value of inundation height for each value of magnitude analyzed.

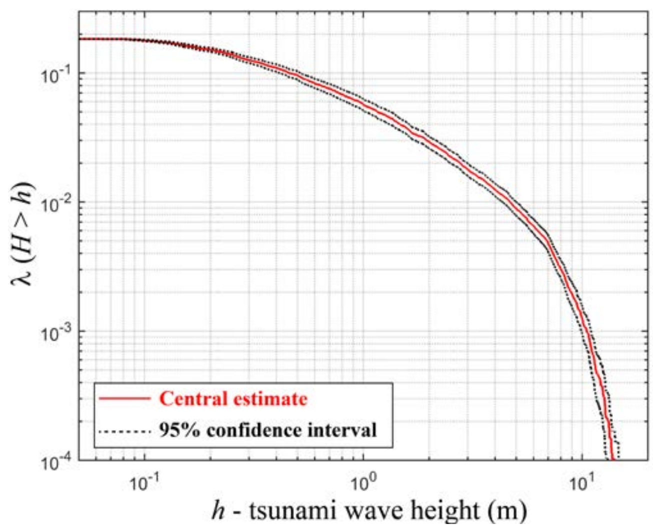

Fig. 6 – Final tsunami hazard curve and the 95% confidence interval.

4. Discussion and Conclusions

A new simulation-based procedure to probabilistically calculate the tsunami hazard for a specific location is presented. The simulation framework allows implementing all potential sources of uncertainties, both epistemic and aleatory. The slip distribution on the fault plane was characterized in detail since it represents the major source of uncertainty. To generate a wide range of earthquake sources, a new generation of scaling relationships specific to subduction zones was used to characterize the tsunami source parameters. For each of seven magnitude values, multiple realizations of possible earthquake slip distribution were generated. The procedure was applied to the Tohoku region, Japan, and a single point located on the coastline of Sendai is considered. For each value of magnitude, 300 tsunami simulations have been performed. The empirical data obtained from the simulations are then used to calculate the empirical CCDF of the tsunami wave height and its confidence interval. Such curves are then combined together with the magnitude-frequency distribution and are summed up in order to obtain the final triplets of hazard curves: one representative of the central estimate and the others corresponding to the 95% confidence interval.

Based on the analysis results, the following conclusions can be drawn:

(a) 300 simulations are sufficient to obtain a reliable and stable representation of the tsunami hazard parameter at a single location, both in terms of central estimates and high percentiles.

(b) For the same number of simulations, passing from small magnitude to large magnitude, there is a reduction of dispersion of the empirical results. That implies a reduction of the confidence interval as well. This is due to the greater variability of the physical earthquake rupture processes for smaller values of magnitude.

(c) The steep slope of the final hazard curve for wave height greater than 10 m (Fig. 6) is the direct consequence of the less variability of tsunami inundation for large values of magnitude.

(d) The confidence interval around the final hazard curves is very tight around the central estimate.

The proposed probabilistic method allows treating all uncertainties involved in the examined natural phenomena. Moreover, the modular structure of the proposed procedure facilitates the extension of the methodology by including the seismic hazard analysis in parallel with the tsunami hazard analysis (but starting from the same earthquake source information). In fact, this work has been extended to a new probabilistic earthquake-tsunami multi-hazard analysis [36].

5. Acknowledgement

This work is funded by the Engineering and Physical Sciences Research Council (EP/M001067/1).

6. References

[1] NGDC, National Geophysical Data Center (NGDC WDS) Global Historical Tsunami Database, Boulder, CO, USA, available at: https://www.ngdc.noaa.gov/hazard/tsu_db.shtml, last access: 31/03/2016.

[2] González FI, Geist EL, Jaffe B, Kânoğlu U, Mofjeld H, Synolakis CE, Titov VV, Arcas D, Bellomo D, Carlton D, Horning T, Johnson J, Newman J, Parsons T, Peters R, Peterson C, Priest G, Venturato A, Weber J, Wong F, Yalciner A (2009). Probabilistic tsunami hazard assessment at Seaside, Oregon, for near-and far-field seismic sources. *Journal of Geophysical Research: Oceans*, **114**, C11023, doi: 10.1029/2008JC005132.

[3] Cheung KF, Wei Y, Yamazaki Y, Yim SC (2011). Modeling of 500-year tsunamis for probabilistic design of coastal infrastructure in the Pacific Northwest. *Coastal Engineering*, **58**(10), 970–985.

[4] Geist EL (2002). Complex earthquake rupture and local tsunamis. *Journal of Geophysical Research: Solid Earth*, **107**(B5), doi: 10.1029/2000JB000139.

[5] Goda K, Mai PM, Yasuda T, Mori N (2014). Sensitivity of tsunami wave profiles and inundation simulations to earthquake slip and fault geometry for the 2011 Tohoku earthquake. *Earth, Planets and Space*, **66**(105), doi: 10.1186/1880-5981-66-105.

[6] Burroughs SM, Tebbens SF (2005). Power-law scaling and probabilistic forecasting of tsunami runup heights. *Pure and Applied Geophysics*, **162**(2), 331-342.

[7] Tinti S, Armigliato A, Tonini R, Maramai A, Graziani L (2005). Assessing the hazard related to tsunamis of tectonic origin: a hybrid statistical-deterministic method applied to southern Italy coasts. *ISET Journal of Earthquake Technology*, **42**, 189–201.

[8] Orfanogiannaki K, Papadopoulos GA (2007). Conditional probability approach of the assessment of tsunami potential: application in three tsunamigenic regions of the Pacific Ocean. *Pure and Applied Geophysics*, **164**(2-3), 593–603.

[9] Geist EL, Parsons T (2006). Probabilistic Analysis of Tsunami Hazards. *Natural Hazards*, **37**(3), 277–314.

[10] Liu Y, Santos A, Wang SM, Shi Y, Liu H, Yuen DA (2007). Tsunami hazards along Chinese coast from potential earthquakes in South China Sea. *Physics of the Earth and Planetary Interiors*, **163**(1), 233–244.

[11] Burbidge D, Cummins PR, Mleczko R, Thio HK (2008). A probabilistic tsunami hazard assessment for Western Australia. *Pure and Applied Geophysics*, **165**(11-12), 2059–2088.

[12] Grezio A, Marzocchi W, Sandri L, Gasparini P (2010). A Bayesian procedure for probabilistic tsunami hazard assessment. *Natural Hazards*, **53**(1), 159–174.

[13] Cornell CA (1968). Engineering seismic risk analysis. *Bulletin of the Seismological Society of America*, **58**(5), 1583–1606.

[14] Houston JR, Garcia AW (1974). Type 16 Flood Insurance Study: Tsunami Predictions for Pacific Coastal Communities. *U.S. Army Engineer Waterways Experiment Station*, Technical Report H-74-3.

[15] Lin IC, Tung CC (1982). A preliminary investigation of tsunami hazard. *Bulletin of the Seismological Society of America*, **72**(6), 2323–2337.

[16] Rikitake T, Aida I (1988). Tsunami hazard probability in Japan. *Bulletin of the Seismological Society of America*, **78**(3), 1268–1278.

[17] Geist EL, Dmowska R (1999). Local tsunamis and distributed slip at the source. *Pure and Applied Geophysics*, **154**, 485–512.

[18] Annaka T, Satake K, Sakakiyama T, Yanagisawa K, Shuto N (2007). Logic-tree Approach for Probabilistic Tsunami Hazard Analysis and its Applications to the Japanese Coasts. *Pure and Applied Geophysics*, **164**(2-3), 577–592.

[19] Thio H K, Somerville P, Ichinose G (2007). Probabilistic analysis of strong ground motion and tsunami hazards in Southeast Asia. *Journal of Earthquake and Tsunami*, **1**(02), 119–137.

[20] Burbidge D, Cummins PR, Mleczko R, Thio HK (2008). A probabilistic tsunami hazard assessment for Western Australia. *Pure and Applied Geophysics*, **165**(11-12), 2059–2088.

[21] Parsons T, Geist EL (2009). Tsunami probability in the Caribbean region. *Pure and Applied Geophysics*, **168**, 2089–2116

[22] Horspool N, Pranantyo I, Griffin J, Latief H, Natawidjaja DH, Kongko W, Cipata A, Bustaman B, Anugrah SD, Thio HK (2014). A probabilistic tsunami hazard assessment for Indonesia. *Natural Hazards and Earth System Science*, **14**(11), 3105–3122.

[23] Mai PM, Beroza GC (2002). A spatial random field model to characterize complexity in earthquake slip. *Journal of Geophysical Research: Solid Earth*, **107**(B11), doi: 10.1029/2001JB000588.

[24] Okada Y (1985). Surface deformation due to shear and tensile faults in a half-space. *Bulletin of the Seismological Society of America*, **75**(4), 1135–1154.

[25] Tanioka Y, Satake K (1996). Tsunami generation by horizontal displacement of ocean bottom. *Geophysical Research Letters*, **23**(8), 861–864.

[26] Goto C, Ogawa Y, Shuto N, Imamura F (1997). Numerical method of tsunami simulation with the leap-frog scheme (IUGG/IOC Time project), IOC Manual, UNESCO, No. 35, Paris, France.

[27] Kaplan EL, Meier P (1958). Nonparametric estimation from incomplete observations. *Journal of the American Statistical Association*, **53**(282): 457–481.

[28] Greenwood M (1926). The natural duration of cancer. Reports on Public Health and Medical Subjects (London: Her Majesty's Stationery Office), **33**, 1–26

[29] Gutenberg B, Richter CF (1956). Magnitude and energy of earthquakes. *Annals of Geophysics*, **9**(1), 1–15.

[30] Headquarters for Earthquake Research Promotion (2013). Investigations of future seismic hazard assessment. 217 p.

[31] Satake K, Fujii Y, Harada T, Namegaya Y (2013). Time and space distribution of coseismic slip of the 2011 Tohoku earthquake as inferred from tsunami waveform data. *Bulletin of the Seismological Society of America*, **103**(2B), 1473–1492.

[32] Fukutani Y, Suppasri A, Imamura F (2016). Stochastic analysis and uncertainty assessment of tsunami wave height using a random source parameter model that targets a Tohoku-type earthquake fault. *Stochastic Environmental Research and Risk Assessment*, **29**(7), 1763–1779.

[33] Mai PM, Thingbaijam KKS (2014). SRCMOD: An online database of finite-fault rupture models. *Seismological Research Letters*, **85**(6), 1348–1357.

[34] Goda K, Yasuda T, Mori N, Maruyama, T (2016). New scaling relationships of earthquake source parameters for stochastic tsunami simulation. *Coastal Engineering Journal*, **58**(3), doi: 10.1142/S0578563416500108.

[35] Lamarre M, Townshend B, Shah HC (1992). Application of the bootstrap method to quantify uncertainty in seismic hazard estimates. *Bulletin of the Seismological Society of America*, **82**(1), 104-119.

[36] De Risi R, Goda K (2016). Probabilistic earthquake-tsunami multi-hazard analysis: application to the Tohoku region, Japan. *Frontiers in Built Environment*, **2**(25), doi: 10.3389/fbuil.2016.00025.